33RD CONGRESS
OF THE INTERNATIONAL COUNCIL
OF THE AERONAUTICAL SCIENCES
STOCKHOLM, SWEDEN, 4-9 SEPTEMBER, 2022

ICAS 2022 SWEDEN

NUMERICAL SIMULATION OF MISSILE AIR-LAUNCHED DYNAMIC PROCESS UNDER DOWNWASH FLOW OF HELICOPTER ROTOR

Zhou Wangyi[1], Yang Guoqiang[1], Gao Xiang[1], Zhu Xueyao[1] & Zhou Boxiao[1]

[1]AVIC Xi' an Flight Automatic Control Research Institute, Xi' an, China, 710065

Abstract

The downwash flow of the helicopter rotor has an important influence on the motion of the missile in the initial stage of air launch, which directly affects the separation safety of the helicopter and missile and the attack precision of the missile. In order to numerically simulate the off-plane process of the missile under the influence of the rotor downwash flow, and to calculate and analyze the motion and trajectory of the missile, this paper develops the unsteady CFD (Computational Fluid Dynamics) numerical method for coupling solution of N-S (Navier-Stokes) equation and 6DoF (six-degree-of-freedom) equation based on the unstructured sliding mesh and dynamic overset mesh technology. Through the calculation of the WPFS (Wing/Pylon/Finned Store) standard model, it is shown that the CFD numerical results are in good agreement with the CTS (Captive Trajectory Simulation Testing) experimental values, which verifies the accuracy and reliability of the developed coupling solution method. On the basis, numerical simulations of the missile air-launching process are carried out in two cases for comparison: with rotor downwash flow and without rotor downwash flow, it reveals that the rotor downwash flow affects the trajectory and attitude of the missile obviously. The study is of great significance for improving the helicopter based launch technology and ballistic control of airborne missiles.

Keywords: rotor downwash flow; missile launch; dynamic overset mesh; multi-body motion; unsteady simulation

1. General Introduction

Armed helicopters can mount rockets, air-to-air missiles, machine guns and other weapon systems for aerial fire strikes. Missiles with helicopters as launch platforms will pass through a strong rotor downwash flow field after leaving the launcher. The initial flight speed of the missile is of the same order of magnitude as the speed induced by downwash flow, and the attitude and trajectory of the missile can be affected by aerodynamic interference, thereby affecting the precision of attacking the target. In order to ensure the separation safety of the helicopter and the missile and improve the attack precision of the missile, it is of great significance to study the aerodynamic interference caused by the downwash flow of helicopter rotor during the process of missile launch. The flow field of helicopter-borne missiles is highly complex, unsteady and nonlinear, including the downwash flow field and the surrounding flow of the missile, along with the inter-interference of the missile, pylon and fuselage. Therefore, it is of important value to carry out the numerical simulation of the dynamic process of air-launched missile under the influence of rotor downwash flow to offer some guidance for the helicopter launch technology.

A few studies have been carried out in this field at home and abroad. Landgrebe [1] calculated the distribution of the downwash flow field of the AH-1G armed helicopter, but the rocket is simplified as a mass point, and the launch orbit is assumed to be a straight line, and the aerodynamic interference of the rotor downwash flow to the rocket is not considered . Zhou Kedong [2] studied the motion law of missiles under the effect of helicopter rotor downwash flow, and gave the influence of downwash flow on the motion of missiles with different launch parameters, but did not analyze the effect on the aerodynamic charicteristics of missile. Wei Jingbiao [3] used the hovering generalized wake model, with the aerodynamic calculation and the initial ballistic calculation coupled, and calculated the aerodynamic characteristics and initial ballistic parameters of the missile under the interference of

rotor downwash flow when the helicopter was hovering.

In order to realize the 6DoF motion simulation of the missile relative to the helicopter after launching in the hovering state, this paper adopts the sliding mesh for the rotating part of the helicopter rotor and the dynamic overset mesh for the moving part of the missile based on the unstructured grid technology, and realizes the coupling solution of N-S equations and 6DOF motion equations, and simulates the motion process of the missile under the comprehensive influence of its own gravity, launch thrust and rotor downwash flow. By comparing the simulation with rotor downwash flow and the simulation without rotor downwash flow, the specific effects of downwash flow on the attitude and trajectory of missile are analyzed, aimed at studying the aerodynamic interference of downwash flow acted on the missile and laying a solid foundation for flight tests.

2. Numerical Methods

2.1 Unstructured Dynamic Overset Mesh Technology

In addition to the rotary motion of the helicopter rotor, there is also the 6DoF motion of the missile during the launch process. Therefore, this paper applies the unstructured dynamic overset mesh technology [4] to simulate the relative motion of the missile and the helicopter. The main idea of the overset mesh technology is to artificially divide the computational flow field into multiple regions. These regions are not isolated, but overlap over the regions. First generate their own mesh in each region, then calculate the flow field, and the calculated data is interpolated through the overset mesh, so that the flow field information of each sub-region is exchanged. The advantage of the overset mesh is that the complex flow field is divided into several relatively simple regions, so the mesh is generated on each region, which improves the speed and quality of mesh generation, and it is convenient for dealing with the relative motion of different objects. The overset mesh generally contains the part of background mesh and the part of overset mesh, which need to be assembled before the calculation of the flow field :

(1)Hole-cutting: this process determines whether the mesh is activated to participate in the flow field calculation, and the overlapping region of overset mesh in the background mesh is divided into active cell type and passive cell type for marking, in which inactive cells do not participate in the calculation of the flow field.

(2) Donor cell search: the first layer of active cells close to passive cells are called acceptor cell or ghost cell. For each acceptor cell, the donor cells of other mesh are required to provide interpolation information.

2.2 N-S Fluid Governing Equations

The governing equation used in this work is the integral form of three dimensional unsteady Navier-Stokes equation [5], as shown in Eq.(1):

$$\frac{\partial}{\partial t}\int_{\Omega}\vec{\boldsymbol{W}}d\Omega+\int_{\Omega}\left(\vec{\boldsymbol{F}}_c-\vec{\boldsymbol{F}}_v\right)ds=\int_{\Omega}\vec{\boldsymbol{Q}}d\Omega \tag{1}$$

Where $\vec{\boldsymbol{W}}$ is the conservative variable vector, $\vec{\boldsymbol{F}}_c$ and $\vec{\boldsymbol{F}}_v$ refer to inviscid flux and viscous flux respectively, $\vec{\boldsymbol{Q}}$ is the source item, their expressions are as follow:

$$\vec{\boldsymbol{W}}=\begin{bmatrix}\rho\\ \rho u\\ \rho v\\ \rho w\\ \rho E\end{bmatrix}\quad \vec{\boldsymbol{F}}_c=\begin{bmatrix}\rho V_r\\ \rho u V_r+pn_x\\ \rho v V_r+pn_y\\ \rho w V_r+pn_z\\ \rho H V_r+pV_b\end{bmatrix}\quad \vec{\boldsymbol{F}}_v=\begin{bmatrix}0\\ \tau_{xx}n_x+\tau_{xy}n_y+\tau_{xz}n_z\\ \tau_{yx}n_x+\tau_{yy}n_y+\tau_{yz}n_z\\ \tau_{zx}n_x+\tau_{zy}n_y+\tau_{zz}n_z\\ \Theta_x n_x+\Theta_y n_y+\Theta_z n_z\end{bmatrix}\quad \vec{\boldsymbol{Q}}=\begin{bmatrix}0\\ \rho f_{e,x}\\ \rho f_{e,y}\\ \rho f_{e,z}\\ \rho\vec{f}_e\cdot\vec{v}+\dot{q}_h\end{bmatrix}$$

Where ρ, p, E, H, $\dot{q}_h$, $\vec{f}_e$ stand for the density, pressure, total energy, total enthalpy, heat transfer coefficient and vector of external force, and u, v, w are the velocity component in x, y, z direction. V_r is the relative velocity between the fluid and overset mesh:

$$V_r=V-V_b$$

$$V=n_x u+n_y v+n_z w$$

$$V_b = n_x u_b + n_y v_b + n_z w_b$$

Where (n_x, n_y, n_z) is the external normal vector of control surface, (u_b, v_b, w_b) is the velocity component of overset mesh in x, y, z direction:

$$\Theta_x = u\tau_{xx} + v\tau_{xy} + w\tau_{xz} + k\frac{\partial T}{\partial x},\ \tau_{xx} = \lambda\left(\frac{\partial u}{\partial x} + \frac{\partial v}{\partial y} + \frac{\partial w}{\partial z}\right) + 2\mu\frac{\partial u}{\partial x},\ \tau_{xy} = \tau_{yx} = \mu\left(\frac{\partial u}{\partial x} + \frac{\partial v}{\partial y}\right)$$

$$\Theta_y = u\tau_{yx} + v\tau_{yy} + w\tau_{yz} + k\frac{\partial T}{\partial y},\ \tau_{yy} = \lambda\left(\frac{\partial u}{\partial x} + \frac{\partial v}{\partial y} + \frac{\partial w}{\partial z}\right) + 2\mu\frac{\partial v}{\partial x},\ \tau_{xz} = \tau_{zx} = \mu\left(\frac{\partial u}{\partial x} + \frac{\partial w}{\partial z}\right)$$

$$\Theta_z = u\tau_{zx} + v\tau_{zy} + w\tau_{zz} + k\frac{\partial T}{\partial z},\ \tau_{zz} = \lambda\left(\frac{\partial u}{\partial x} + \frac{\partial v}{\partial y} + \frac{\partial w}{\partial z}\right) + 2\mu\frac{\partial w}{\partial x},\ \tau_{yz} = \tau_{zy} = \mu\left(\frac{\partial v}{\partial y} + \frac{\partial w}{\partial z}\right)$$

Where μ and λ are the dynamic viscosity coefficient and the second viscosity coefficient，k is heat transfer coefficient. Under the Stokes assumption $\lambda = -\frac{2}{3}\mu$. In addition to the above basic governing equations, three additional equations need to be added, and the equation system can be closed:

$$p = p(\rho, T) \tag{2}$$

$$p = (\gamma - 1)\rho\left[E + \frac{1}{2}\left(u^2 + v^2 + w^2\right)\right] \tag{3}$$

$$H = E + \frac{p}{\rho} \tag{4}$$

The finite volume method is used to solve the the density-based continuous, momentum and energy equations with fully coupled algorithm. The Roe scheme [6] with flux differential splitting is adopted, the viscous flux adopts the Jameson central difference scheme [7], and the time discretization adopts the implicit double-timestep method [8]. The k-ε turbulence model [9] is selected.

2.3 6 DoF Motion Equations

Regardless of the rotation of the earth and the aero-elastic deformation of the missile, the 6DOF dynamic equations of motion can be described by the following twelve first-order differential equations:

$$\dot{u} = vr - wq - g\sin\theta + \frac{F_x}{m} \tag{5}$$

$$\dot{v} = -ur + wp + g\cos\theta\sin\phi + \frac{F_y}{m} \tag{6}$$

$$\dot{w} = uq - vp + g\cos\theta\cos\phi + \frac{F_z}{m} \tag{7}$$

$$\dot{\phi} = p + (r\cos\phi + q\sin\phi)\tan\theta \tag{8}$$

$$\dot{\theta} = q\cos\phi - r\sin\phi \tag{9}$$

$$\dot{\psi} = \frac{1}{\cos\theta}(r\cos\phi + q\sin\phi) \tag{10}$$

$$\dot{p} = (c_1 r + c_2 p)q + c_3 L + c_4 N \tag{11}$$

$$\dot{q} = c_5 pr - c_6(p^2 - r^2)q + c_7 M \tag{12}$$

$$\dot{r} = (c_8 p - c_2 r)q + c_4 L + c_9 N \tag{13}$$

$$\dot{x}_g = u\cos\theta\cos\psi + v(\sin\phi\sin\theta\cos\psi - \cos\phi\sin\psi) + w(\sin\phi\sin\psi + \cos\phi\sin\theta\cos\psi) \tag{14}$$

$$\dot{y}_g = u\cos\theta\sin\psi + v(\sin\phi\sin\theta\sin\psi + \cos\phi\cos\psi) + w(-\sin\phi\cos\psi + \cos\phi\sin\theta\sin\psi) \tag{15}$$

$$\dot{h} = u\sin\theta - v\sin\phi\cos\theta - w\cos\phi\cos\theta \tag{16}$$

Where $c_1 = \frac{(I_y - I_z)I_z - I_{xz}^2}{\sum}$, $c_2 = \frac{(I_x - I_y + I_z)I_{xz}}{\sum}$, $c_3 = \frac{I_z}{\sum}$, $c_4 = \frac{I_{xz}}{\sum}$, $c_5 = \frac{I_z - I_x}{I_y}$, $c_6 = \frac{I_{xz}}{I_y}$, $c_7 = \frac{1}{I_y}$,

$c_8 = \frac{I_x(I_x - I_y) + I_{xz}^2}{\sum}$, $c_9 = \frac{I_x}{\sum}$, $\sum = I_x I_z - I_{xz}^2$.

Where u, v, w represents the three-axis speed; ϕ, θ, ψ stands for the roll angle, pitch angle and heading angle; p, q, r represents the three-axis angular rate; x_g, y_g, h represents the ground displacement; F_x, F_y, F_z represents the three-axis force; L, M, N represents the three-axis torque.

2.4 Coupling Solution of N-S Equations and 6DoF Equations

The coupling solution of rigid body and fluid is carried out as follows:

(1)Solve the fluid governing equations at (initial time) to obtain the parameters of the flow field. Integrate the surface pressure of the moving object to obtain the total force and total moment;

(2)Calculate the acceleration of the center of mass at from the motion equation Eq.(5)-Eq.(7), and integrate it with time to obtain the relative velocity and relative displacement of the center of mass;

(3)Calculate the angular acceleration around the center of mass at from the motion equations Eq.(11)-Eq.(13), and integrate with time to obtain the angular velocity and angle around the center of mass;

(4)According to the calculated the displacement of the center of mass and the angle around the center of mass at time , update the position information of overset mesh. At the same time, the time advances one step further;

(5)Return to step (1) and recalculate the next time step.

Figure 1 shows the coupling solution process of the N-S equations and the 6DoF equations.

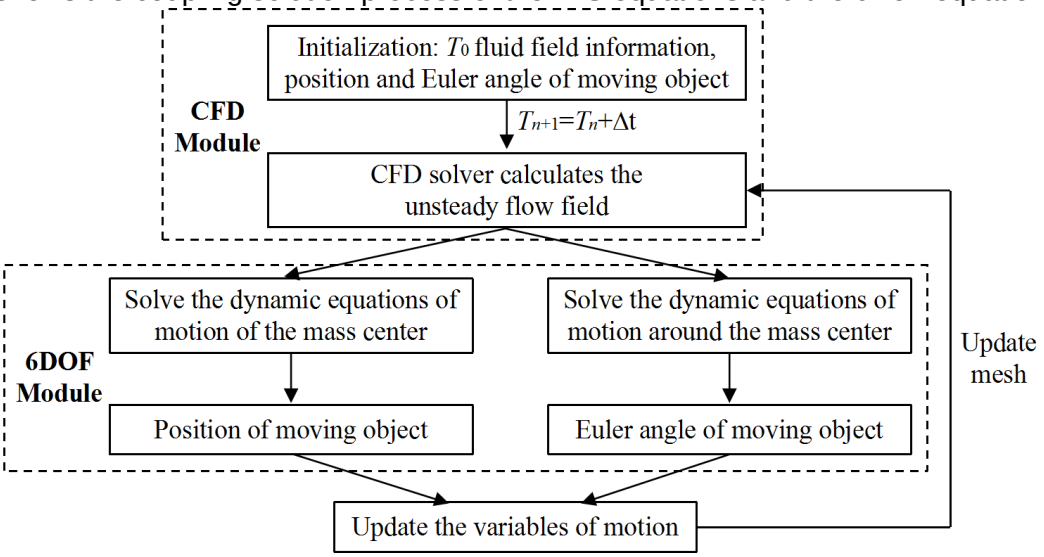

Figure 1 – The coupling solution process of the N-S equations and the 6DoF equations.

3. Validation numerical example

The three-dimensional WPFS model is selected to verify the numerical method for the coupling solution of the N-S equations and the 6DoF equations. Funded by the U.S. AFRL (Air Force Research Laboratory), the AEDC (Arnold Engineering Development Center) completed its CTS test, and acquired detailed and reliable experiments data[10], which has become the benchmark for the validation of the effectiveness of the numerical simulation for aircraft multi-body separation. The parameters related to the wing, pylon, missile and ejection force are shown in table 1 and table 2.

Table 1 – Geometric parameters of wing and pylon.

Geometric parameter	Value
Sweep angle of leading edge (deg)	45

Sweep angle of trailing edge (deg)	0
Chord length of wing root (mm)	7620
Airfoil of wing	NACA64A010
Half span of wing (mm)	6600
Aspect Ratio of wing	1.73
Geometric size of pylon (mm)	2200*150* 610

Table 2 – Parameters of missile and its ejection force.

Parameter	Value
Mass (kg)	907
Reference length (mm)	3017.5
Reference diameter (mm)	500
Airfoil of tail	NACA0008
Position of mass center (mm)	1417
Moment of inertia *Ixx*/*Iyy*/*Izz* (kg • mm^3)	27/488/488
Position of front ejection force (mm)	1237.5
Front ejection force (kN)	10.7
Position of rear ejection force (mm)	1746.5
Rear ejection force (kN)	42.7
Action time of ejection force (s)	0.054

Figure 2 shows the surface mesh of the WPFS model. The calculation condition is: *Ma*=1.2, *H*=11600m, *α*=0°. Take the steady flow field as the initial value of the unsteady flow field, and then release the missile, calculate the trajectory and attitude of the missile. The length of unsteady time step is *Δt*=0.005s, and the number of total step is 160, that is the physical time of falling process of the missile within 0.8s.

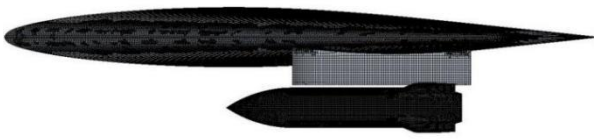

Figure 2 – The surface mesh of the WPFS model.

Figure 3 shows the trajectory of the missile at different time moments within 0.8s. In addition to the pitch moment generated by the downwash flow of the wing, the missile is also affected by the sidewash flow of the wing. The aerodynamic layout of wing is the swept delta wing, so the airflow along the lower surface of the wing eventually evolves into sidewash flow, thus the missile is subjected to lateral aerodynamic force and generates yaw moment. The asymmetrical aerodynamic force generated by the wing will also cause the missile to roll to some extent.

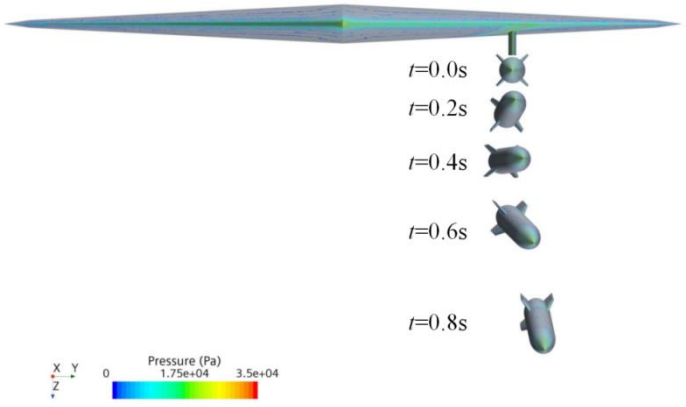

(a) Front view

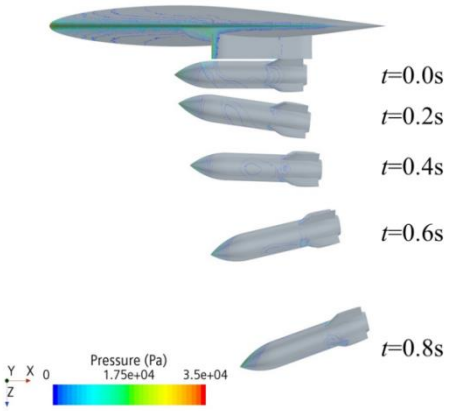

(b) Side view

Figure 3 – The trajectory of the missile at different time moments within 0.8s.

Figure 4 show the comparison between the CFD calculated values and the CST experimental values of displacement, velocity, Euler angle and angular velocity within t=0~0.8s. It shows that the CFD data and CST data are in good agreement, and the numerical method applied can effectively simulate the separation and motion of missile.

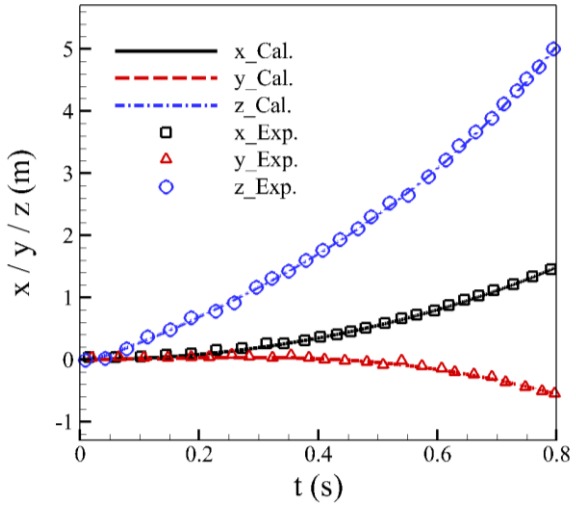

(a) Displacement

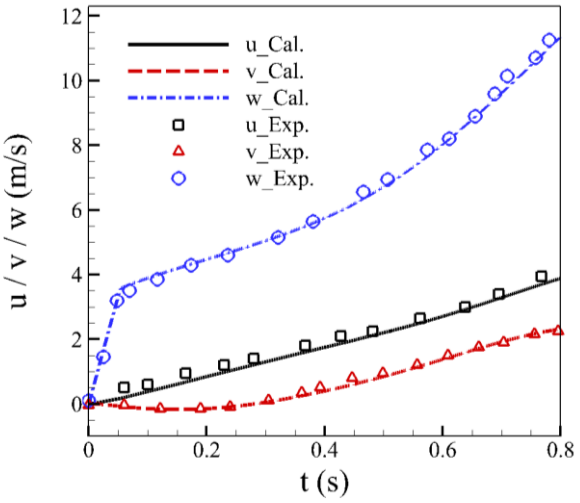

(b) Velocity

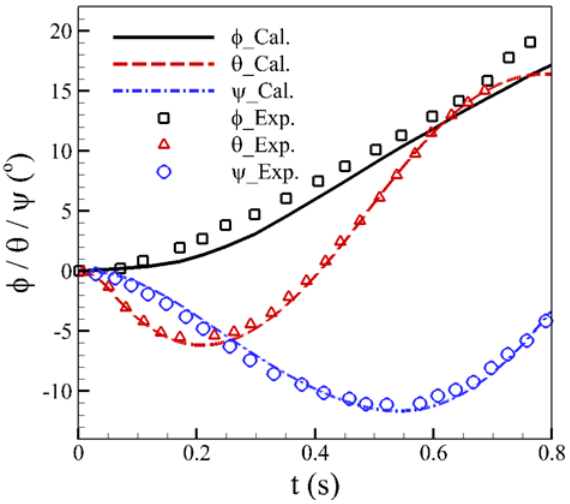

(c) Euler angle

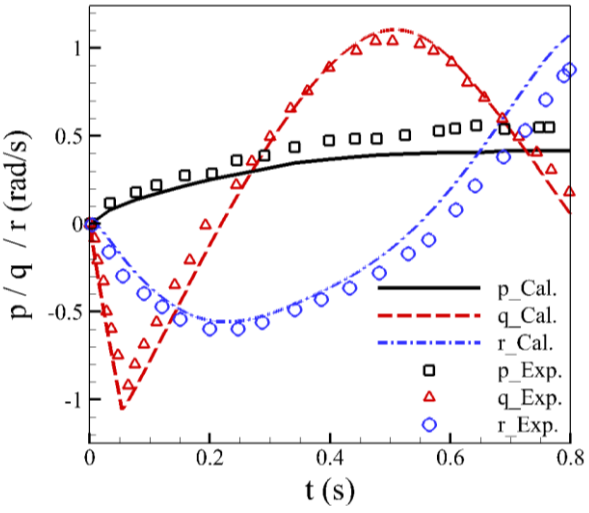

(d) Angular velocity

Figure 4 – The comparison between CFD and CST data.

4. Simulation of air-launch missile under downwash flow of helicopter rotor

The Robin rotor/fuselage combination model [11] is selected as the helicopter model, including four

blades and a fuselage. The geometric parameters of helicopter are shown in Table 3. The missile model uses the air-to-air missile with conventional layout, and its geometric parameters are shown in Table 4. The combination model of the helicopter and missile used for calculation is shown in Figure 5. The rotor hub, launch pylon and other components are not considered.

Table 3 – Geometric parameters of helicopter.

Parameter	Value
Rotor diameter (m)	17
Rotor airfoil	NASA RC10-(B) M002
Rotor speed (r/min)	300

Table 4 – Geometric parameters of missile.

Parameter	Value
Mass (kg)	40
Reference length (m)	2.5
Center of mass position (m)	1.0
Moment of inertia *Ixx* /*Iyy* /*Izz* (kg • m^2)	0.52/22/21
Initial velocity (m/s)	0
Initial angular velocity (deg/s)	0
Thrust magnitude (N)	3920
Thrust direction	X

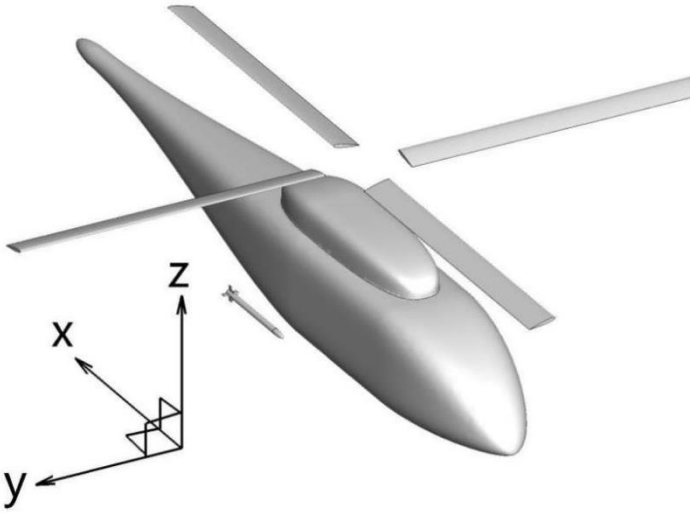

Figure 5 – The combination model of the helicopter and missile.

The helicopter and missile combination model is divided into three computational domains, including the rotation domain of the helicopter rotor, the motion domain of the launched missile and the static domain of the helicopter body, as shown in Figure 6. The rotation domain applies the sliding mesh, and the motion domain adopts the dynamic overset mesh, and the total amount of generated mesh is 15 million. Figure 7 displays the mesh distribution of the model.

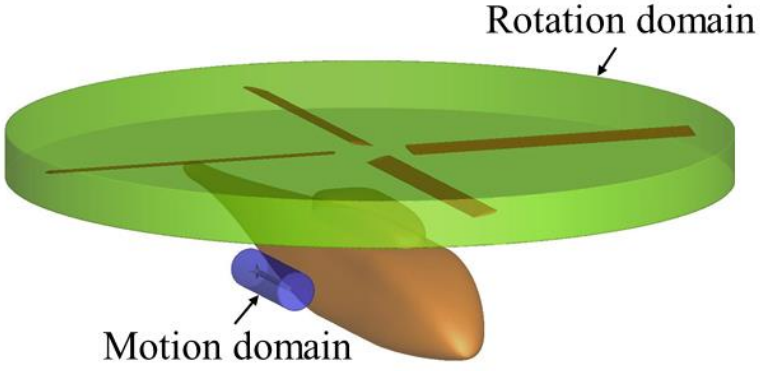

Figure 6 – Three divisions of the computational domain.

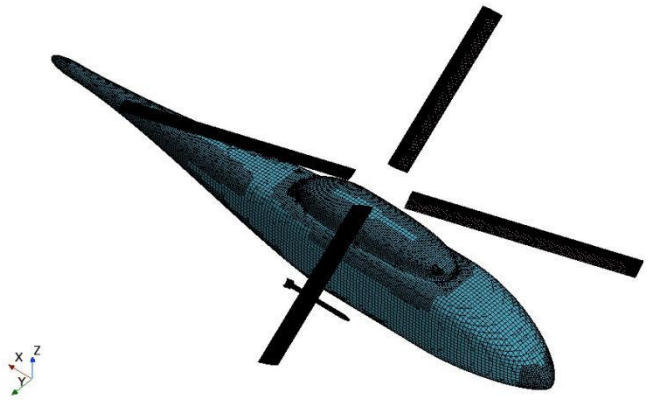

(a) Surface mesh

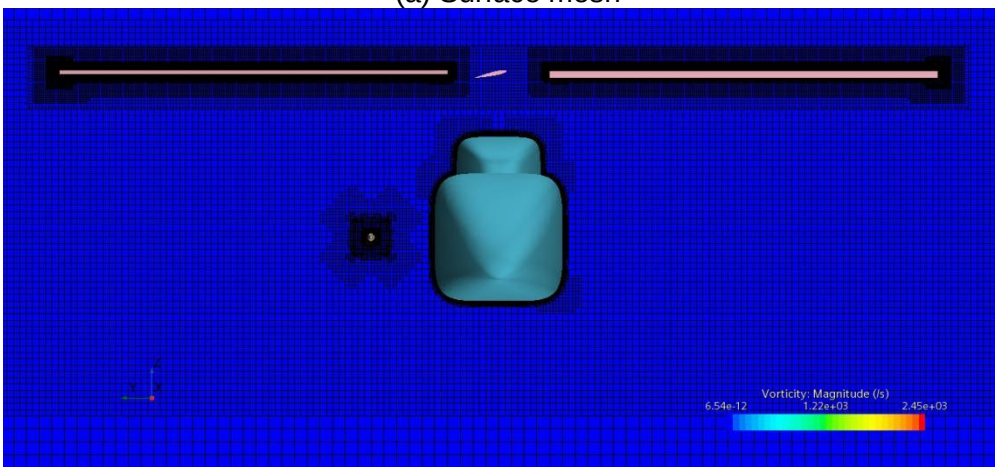

(b) Spatial mesh

Figure 7 – Displays the mesh distribution of the model.

The specific conditions and settings of the calculation are shown in Table 5.

Table 5 – The specific conditions and settings of the calculation.

Parameter	Value
Helicopter status	Hover
Flight height (m)	100
Angle of attack (deg)	0
Physical time step (s)	0.001
Sub-iteration steps	30
Total physical time (s)	0.7

In order to analyze the influence of rotor downwash flow on the missile launch process, under the premise of other calculation conditions being consistent, the calculation is divided into two cases: the helicopter rotor without rotation (without downwash flow) and helicopter rotor with rotation (with downwash flow). Under the thrust of 10 times gravity, the time for the missile to leave the region of downwash flow field is about 0.45s. Figure 8 and Figure 9 are the top view and side view of the missile launch trajectory without and with rotor downwash flow respectively. It can be seen that under the action of the downwash flow, the pitch angle of the missile gradually increases, and generates a rightward yaw angle after leaving the region of downwash flow.

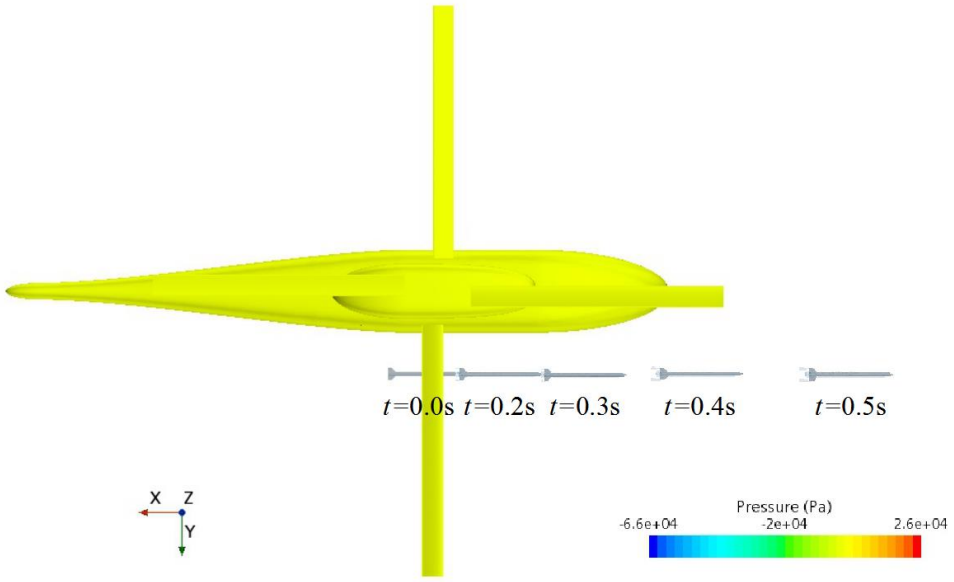

(a) Without rotor downwash flow

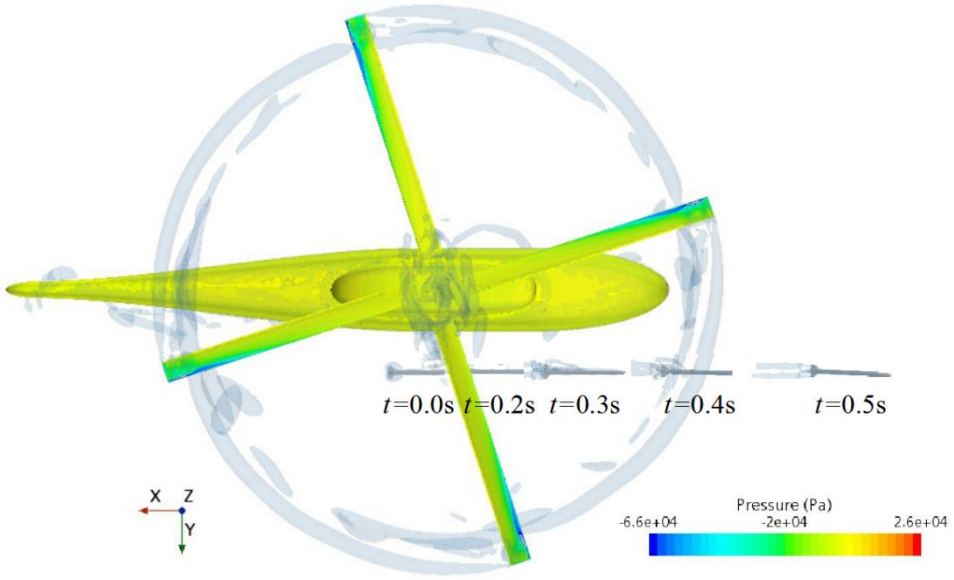

(b) With rotor downwash flow

Figure 8 – Top view of missile launch trajectory.

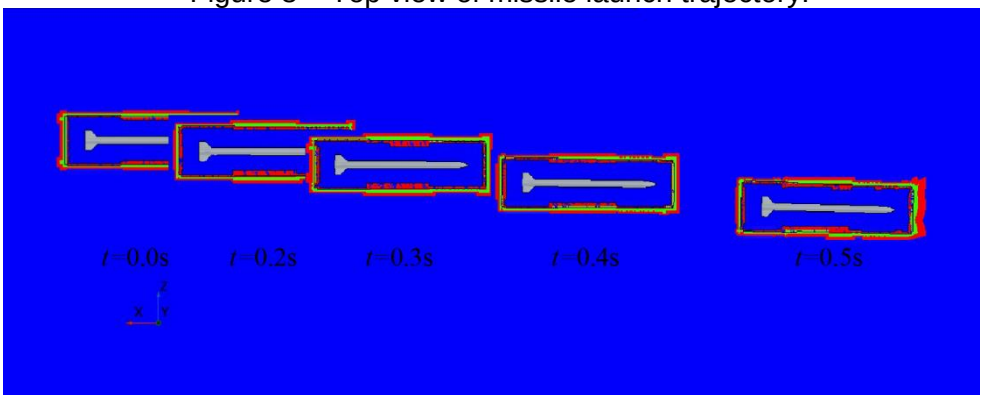

(a) Without rotor downwash flow

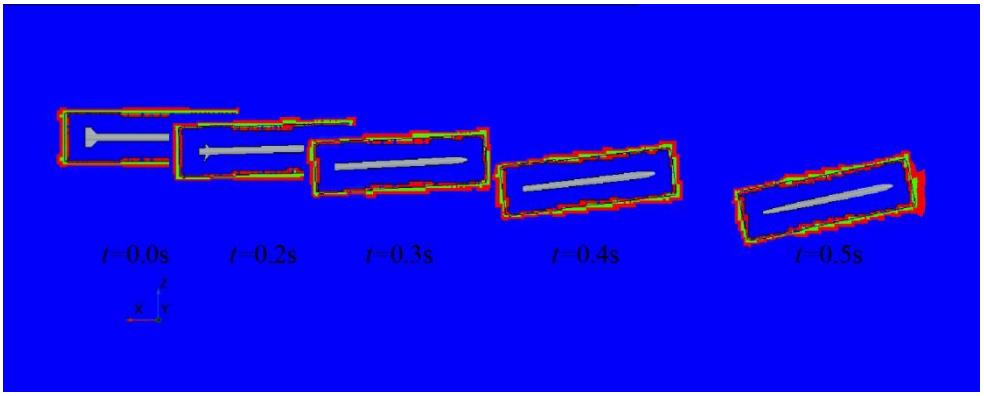

(b) With rotor downwash flow

Figure 9 – Side view of missile launch trajectory.

Figure 10- Figure 13 show the comparison curves of the displacement, velocity, Euler angle and angular velocity of the missile with and without downwash flow within time t=0~0.5s. It shows that the rotor downwash flow has little effect on the displacement and velocity of the missile because the x-direction of the missile body is subjected to a thrust of 10 times gravity, which is much greater than the aerodynamic interference caused by the downwash flow. Under the influence of the unsteady and asymmetric rotor downwash flow, the four tail fins of missile generate left roll angle, head-up pitch angle and right yaw angle. Especially in the vicinity of detachment of downwash flow, the pitch angle is up to 10° .

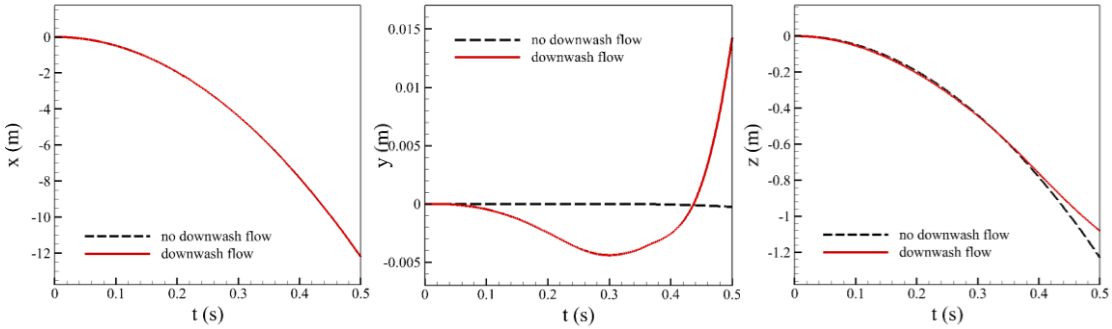

(a) X-direction displacement (b) Y-direction displacement (c) Z-direction displacement

Figure 10 – Comparison of the displacement with and without downwash flow.

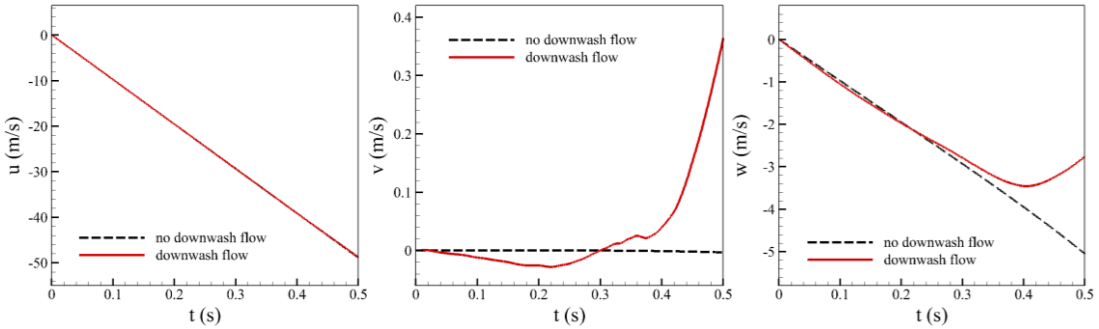

(a) X-direction velocity (b) Y-direction velocity (c) Z-direction velocity

Figure 11 – Comparison of the velocity with and without downwash flow.

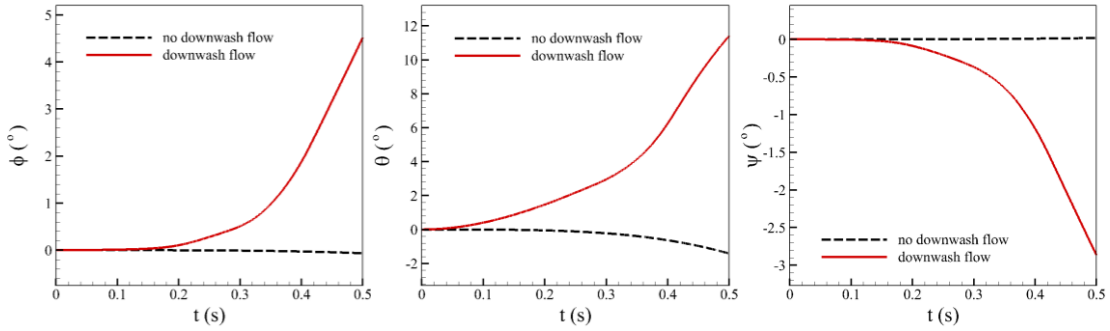

(a) Roll angle (b) Pitch angle (c) Yaw angle

Figure 12 – Comparison of the Euler angle with and without downwash flow.

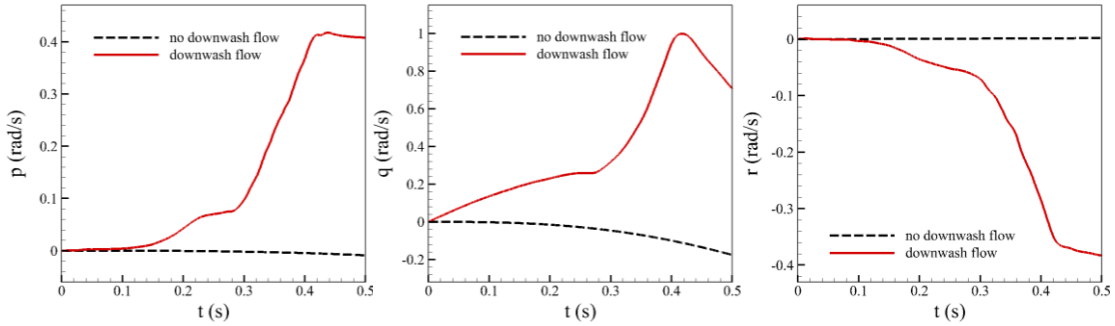

(a) Roll angular velocity (b) Pitch angular velocity (c) Yaw angular velocity

Figure 13 – Comparison of the angular velocity with and without downwash flow.

Figure 14 and Figure 15 are the pressure distribution of the missile surface without and with downwash flow at t=0.36s, respectively. When there is no downwash flow, the pressure on the missile surface is almost symmetrically distributed, and the pressure changes gently; when there is downwash flow, the upper surface of the missile appears local high pressure, and the side surface shows local low pressure. Due to the uneven pressure distribution, the missile possesses asymmetrical forces and moments, which in turn affect the trajectory and attitude of the missile.

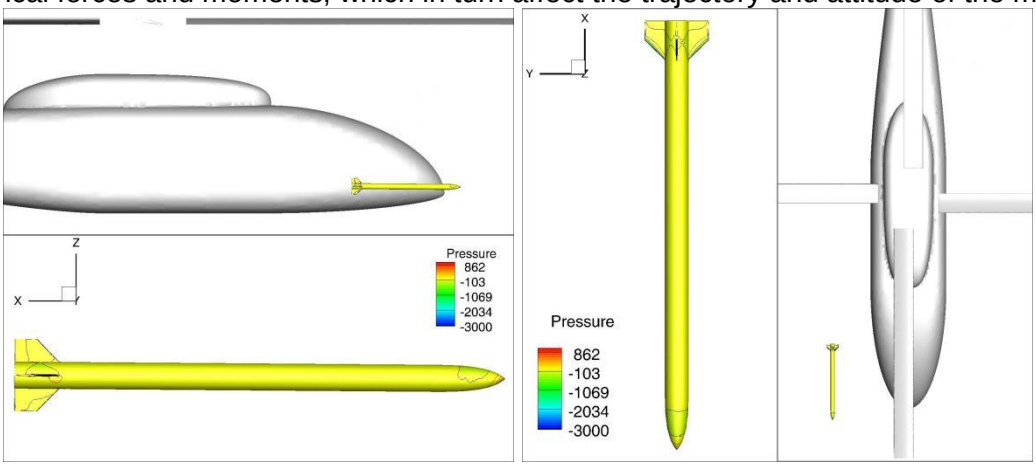

(a) Side view (b) Top view

Figure 14 – Missile surface pressure distribution without downwash flow at t=0.36s.

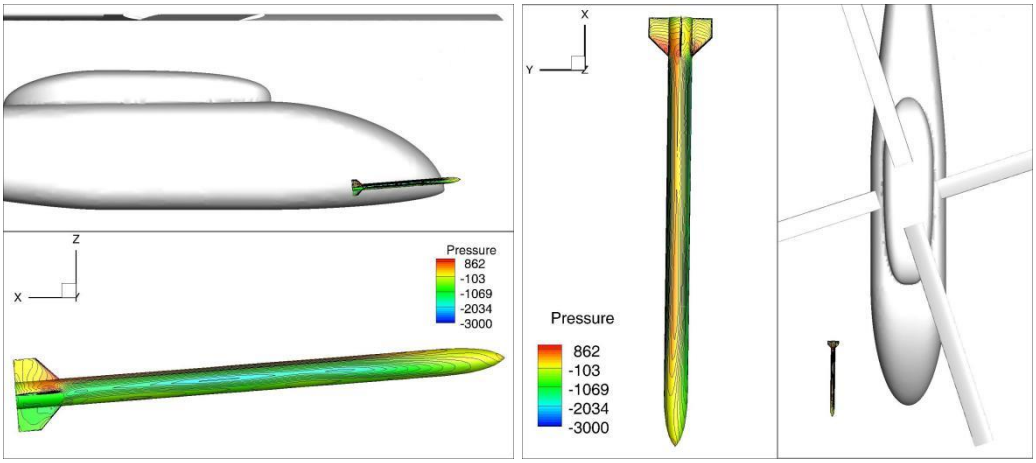

(a) Side view (b) Top view

Figure 15 – Missile surface pressure distribution with downwash flow at t=0.36s.

Figure 16 and Figure 17 are the spatial pressure and velocity distribution of the missile without and with downwash flow at t=0.36s, respectively. In the absence of downwash flow, the disturbance of flow field is only produced by the moving missile. When the helicopter rotor rotates, a highly rotating downwash flow field is generated in the horizontal plane; in the vertical plane, a downward downwash velocity is generated, and downward-moving tip vortex is continuously generated around the tip of the rotor. The downwash speed near the rotor tip is as high as 50m/s, which is close to the moving speed of the missile. Through the analysis of the flow field, it can be revealed that the highly unsteady and nonlinear characteristics of the rotor downwash flow are the main reasons for the change of the trajectory and attitude angle of air-launched missile.

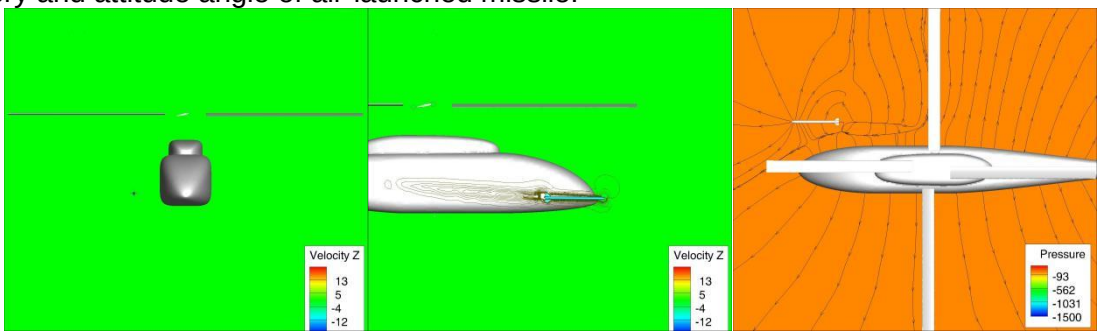

(a) Front view (b) Side view (c) Top view

Figure 16 – Spatial pressure and velocity distribution without downwash flow at t=0.36s.

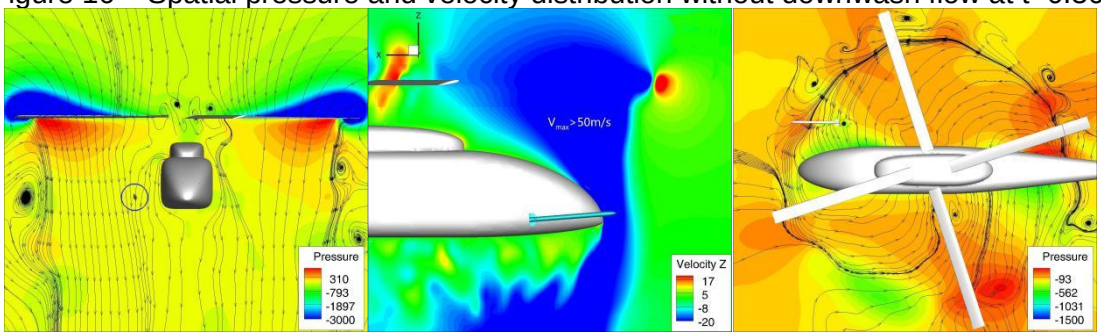

(a) Front view (b) Side view (c) Top view

Figure 17 – Spatial pressure and velocity distribution with downwash flow at t=0.36s.

5. Conclusion

In this paper, an unsteady CFD numerical method with coupled solution of N-S equations and 6DoF equations based on slip mesh and dynamic overset mesh technology is developed. By comparing the CFD calculated values with the CTS experimental values of the WPFS model, the two values are in good agreement, which verifies the accuracy and reliability of the mentioned numerical method. Carry out study on the effect of rotor downwash flow on motion process the air-launched missile. By comparing the spatial flow field, the surface pressure distribution, the movement trajectory and attitude of the missile, the results conclude that under the comprehensive action of the gravity, thrust

of booster and rotor downwash flow, the missile can realize safe separation from the helicopter, but addition attention should be paid to attitude control after the missile leaves the region of downwash flow field.

6. Contact Author Email Address

Corresponding author: Zhou Wangyi, Email address: 1208210734@qq.com

7. Copyright Statement

References

[1] ANTONJL. Prediction of rotor wake induced flow along the rocket trajectories of an army AH-1G helicopter[R]. AD A007878, 1975.

[2] ZHOU Kedong, etal. A study on the movement of rocket under down-wash flow of a helicopter's rotor[J]. ACTA ARMAMENTAR, 2003, 24(2): 204-208.

[3] Wei Jingbiao, Xue Xiaozhong. Aerodynamic characteristics and initial ballistic interference on a missile by a helicopter's rotor down-wash in hovering[J]. ACTA AERODYNAMICA SINICA, 2005, 23(2): 217-221.

[4] Togashi F, Ito Y, Nakahashi K, Obayashi S. Overset Unstructured Grids Method for Viscous Flow[J].Computations. AIAA Journal, 2006, 44(7): 1617-1623.

[5] Teman, R. Navier-Stokes equations : theory and numerical analysis, 1977.

[6] Roe P L. Approximate Riemann solvers, parameter vectors, and difference schemes[J]. Journal of Computational Physics, 1981, 43(2):357-372.

[7] Blazek J, Blazek J. Computational Fluid Dynamics: Principles and Applications, Second Edition[J]. Computational Fluid Dynamics Principles & Applications, 2005, 55(2):1-4.

[8] Yan Chao. Computational fluid dynamics method and application[M]. Press of BUAA, 2006.

[9] Versteeg H K, Malalasekera W. An introduction to computational fluid dynamics - The finite volume method[M]. Press company of world library, 2000:400.

[10]Heim E R. CFD Wing/Pylon/Finned Store Mutual Interference Wind Tunnel Experiment[J]. AEDC-TSR-91-P4, 1991.

[11]Freeman, C.E., Mineck.R.E. Fuselage surface pressure measurements of a helicopter wind-tunnel model with a 3.15meter diameter single rotor[R]. NASA Technical Memorandum, N79-26015, 1979.